Discrimination between Winter Precipitation Types Based on Spectral-Bin Microphysical Modeling

HEATHER DAWN REEVES, ALEXANDER V. RYZHKOV, AND J. KRAUSE

*Cooperative Institute for Mesoscale Meteorological Studies, University of Oklahoma, and
NOAA/OAR/National Severe Storms Laboratory, Norman, Oklahoma*

ABSTRACT

A new approach for distinguishing precipitation types at the surface, the spectral bin classifier (SBC), is presented. This algorithm diagnoses six categories of precipitation: rain (RA), snow (SN), a rain–snow mix (RASN), freezing rain (FZRA), ice pellets (PL), and a freezing rain–ice pellet mix (FZRAPL). It works by calculating the liquid-water fraction f_w for a spectrum of falling hydrometeors given a prescribed temperature T and relative humidity profile. Demonstrations of the SBC output show that it provides reasonable estimates of f_w of various-sized hydrometeors for the different categories of precipitation. The SBC also faithfully represents the horizontal distribution of precipitation type inasmuch as the model analyses and surface observations are consistent with each other. When applied to a collection of observed soundings associated with RA, SN, FZRA, and PL, the classifier has probabilities of detection (PODs) that range from 62.4% to 98.3%. The PODs do decrease when the effects of model uncertainty are accounted for. This decrease is modest for RA, SN, and PL but is large for FZRA as a result of the fact that this form of precipitation is very sensitive to small changes in the thermal profile. The effects of the choice of the degree of riming above the melting layer, the drop size distribution, and the assumed temperature at which ice nucleates are also examined. Recommendations on how to mitigate all forms of uncertainty are discussed. These include the use of dual-polarized radar observations, incorporating output from the microphysical parameterization scheme, and the use of ensemble model forecasts.

1. Introduction

An accurate analysis and prediction of precipitation type during winter is one of the greatest challenges facing forecasters today (Ralph et al. 2005; Stewart et al. 2015). While numerous algorithms exist to determine the surface precipitation type, most have strong biases that impede their ability to correctly distinguish freezing rain from ice pellets (FZRA and PL; e.g., Reeves et al. 2014; Elmore et al. 2015). Ryzhkov et al. (2014) demonstrated that by explicitly calculating the liquid-water fraction of falling hydrometeors for a spectrum of drop sizes one can more accurately discriminate FZRA and PL. Herein, their approach is expanded and tested for a wide variety of environments. Results show this algorithm reliably detects both FZRA and PL as well as rain and snow (RA and SN).

Corresponding author address: Heather Dawn Reeves, NOAA/ National Severe Storms Laboratory, Ste. 2401, 120 David L. Boren Blvd., Norman, OK 73072-7319.
E-mail: heather.reeves@noaa.gov

The surface precipitation type is controlled by several factors including the drop size distribution (DSD), precipitation rate, hydrometeor interactions, and the initial-phase composition of the hydrometeor (Crawford and Stewart 1995; Bernstein 2000; Cortinas 2000; Rauber et al. 2000, 2001; Robbins and Cortinas 2002; Changnon 2003; Cortinas et al. 2004; Thériault et al. 2010). However, it is generally believed that the primary dictator is the vertical distribution of the wet-bulb temperature T_w (e.g., Bourgouin 2000). As a consequence, a number of algorithms have been devised that solely rely on the T_w profile to determine the precipitation type (e.g., Ramer 1993; Baldwin et al. 1994; Bourgouin 2000; Schuur et al. 2012). While computationally efficient and good at detecting SN and RA, most such algorithms have been found to be rather poor at discriminating either or both of FZRA and PL (Bourgouin 2000; Manikin et al. 2004; Manikin 2005; Wandishin et al. 2005; Reeves et al. 2014; Elmore et al. 2015). Reeves et al. (2014) found the cause of these errors to be faulty assumptions about what characteristics in the T_w profiles distinguish FZRA from PL. They were unable to find any set of characteristics in
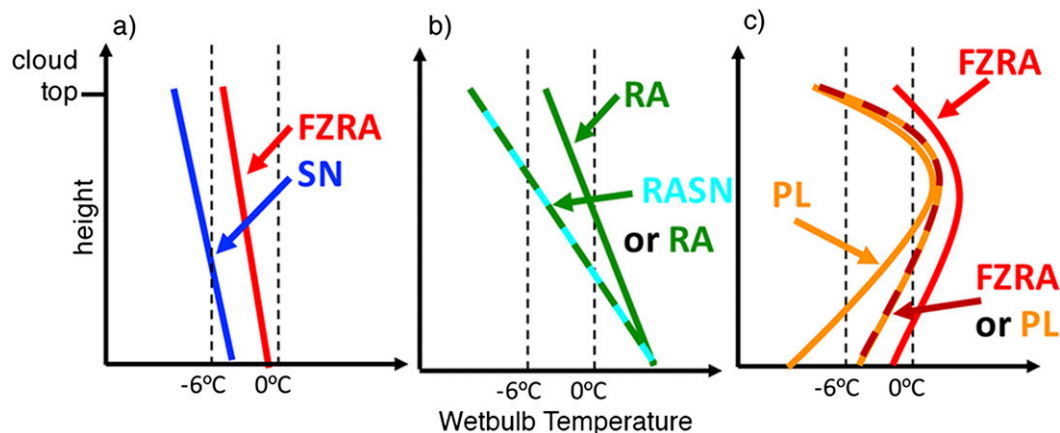
FIG. 1. Idealized profiles of wet-bulb temperature assuming (a) no, (b) one, and (c) two crossings of the 0°C isotherm. The possible precipitation types for each profile are indicated.

the profiles that can be used to reliably discriminate FZRA from PL, suggesting microphysical controls may be more important than previously thought.

One could account for microphysical effects by using the model-predicted mixing ratios of SN, RA, and graupel, but this approach has certain limitations. For example, microphysics schemes used in operational models do not allow for mixed-phase hydrometeors, an important control on the surface precipitation type (Thériault and Stewart 2010). Also, there are no existing schemes that allow for a PL category. Therefore, when a hydrometeor refreezes, it is converted to either SN, graupel (i.e., Thompson et al. 2014), or hail. This makes the unambiguous discrimination between SN and PL quite challenging. We also note that comparisons between algorithms that use model-diagnosed hydrometeor habits and those that utilize only T_w profiles yield similar statistics (Ikeda et al. 2013; Reeves et al. 2014; Elmore et al. 2015; Benjamin et al. 2016), indicating this approach is not necessarily a superior one. Since hydrometeor mixing ratios at the surface are not routinely measured, the diagnosis and correction of systematic errors in this type of algorithm is difficult.

Hybrid methods that blend microphysical information and sounding data have been proposed. Ramer (1993) introduced a technique to assign the liquid-water content of hydrometeors as they fall from the so-called precipitation-generation layer to the surface. Reeves et al. (2014) found this algorithm performs very poorly at detecting PL because of poor assumptions about how the liquid-water fraction is related to T_w. Czys et al. (1996) promoted a more sophisticated approach that uses an assumed terminal velocity of a hypothetical

hydrometeor and the depth of elevated warm layers to discriminate between FZRA and PL. However, Rauber et al. (2001) argue this method is not effective since it assumes hydrometeors are completely frozen at the cloud top, an assumption that can lead to erroneous classifications when untrue. All of the above algorithms are built upon the assumption of a single hydrometeor size that may not be representative of the actual median drop size, another likely contributor to errant diagnoses.

A potentially viable method is to explicitly compute the rates of melting and refreezing for a spectrum of drop sizes. Such an algorithm is described and tested herein and is henceforth referred to as the spectral bin classifier (SBC). A description of the SBC and demonstration of its performance for select soundings are provided in section 2. A statistical assessment of the SBC along with consideration of the effects of various sources of uncertainty is presented in section 3. Concluding thoughts are discussed in section 4.

2. Algorithm logic and design

a. Thermal and microphysical controls in the surface precipitation type

Consider the three thermal profile types in Fig. 1. The simplest are the completely subfreezing profiles shown in Fig. 1a. The surface precipitation type for these profiles is dictated by whether the cloud-top wet-bulb temperature T_{w-ct} is less than the ice nucleation temperature T_{ice}. We define T_{ice} as the wet-bulb temperature at which the ice nucleus in a water droplet becomes activated (usually less than -5°C; e.g., Meyers et al.

1992; Petters and Wright 2015). If $T_{w-ct} \leq T_{ice}$, ice crystals will form and the resulting surface precipitation type will be SN. Otherwise, supercooled liquid-water droplets will form, resulting in FZRA.

The profiles in Fig. 1b cross the 0°C isotherm one time and have surface T_ws that are greater than 0°C. If $T_{w-ct} > T_{ice}$, only liquid-water droplets will form aloft and these will simply warm to above-freezing temperatures as they enter the melting layer, yielding RA at the surface. If not, the precipitation type will depend on whether the frozen particles entering the melting layer have sufficient time to completely melt before reaching the surface. The larger and more heavily rimed a particle is, the more time it will require to completely melt. Therefore, for this condition, one may have fully melted liquid-water drops at the surface, resulting in RA, or partially melted ice particles. This latter class is sometimes referred to as wet snow, but the official Automated Surface Observing Station (ASOS) record will indicate RASN, which stands for a RA–SN mix. We use the terminology RASN throughout the rest of the paper.

The third profile type has an elevated warm layer capping a surface-based subfreezing layer (Fig. 1c). Assuming the cloud top is above the highest crossing of the 0°C isotherm, there are two possible precipitation types. If all hydrometers completely melt in the melting layer or $T_{w-ct} > T_{ice}$, the subfreezing layer will require $T_w \leq T_{ice}$ for ice nucleation and refreezing to occur. If this condition is met and the droplets refreeze before reaching the ground, PL will be observed. Otherwise, the precipitation type will be FZRA. If the melting layer is sufficiently cool and shallow or the hydrometeors sufficiently large and rimed before entering it, they may not completely melt. In this case, the hydrometeors will have active ice nuclei and refreezing will begin immediately when the hydrometeors enter the subfreezing layer, resulting in PL. It is possible, given a spectrum of drop sizes, for multiple phases (some frozen, some liquid) to occur in the same volume, yielding a mixture of FZRA and PL. This mixture is referred to as FZRAPL. More complex soundings, with multiple melting and refreezing layers, are possible. Depending on the surface T_w, FZRA, PL, or RA, or some combination of the three, may be observed.

When one considers both the thermal and microphysical forcings, as above, it is clear that an accurate discrimination of the precipitation type requires knowledge of the drop size, the amount of riming on hydrometeors above the melting layer, and the amount of liquid water in the hydrometeors as they enter near-surface subfreezing layers. One must also properly designate the phase of the hydrometer at the cloud top, as argued by Rauber et al. (2001). To the best of our knowledge, there are no existing algorithms that account for all of these controls.

b. Methodology

Herein, a new algorithm is described and tested. This algorithm, referred to as the spectral bin classifier, is a one-dimensional spectral-bin model that calculates the liquid-water fraction f_w for a spectrum of hydrometeor sizes and, therefore, can account for the above microphysical controls. It follows the logic described in Ryzhkov et al. (2014) with some alterations. Namely, it diagnoses six (rather than four) categories of precipitation: SN, RA, FZRA, PL, RASN, and a FZRA–PL mix (FZRAPL). Other modifications include 1) assigning the hydrometeor phase at the cloud top rather than assuming it is frozen, 2) allowing for multiple melting and refreezing layers, and 3) further refinement of the conditions that are used to discriminate between FZRA and PL.

The effectiveness and sensitivity of the SBC is demonstrated in several different ways. This includes examination of profiles of f_w across the hydrometeor spectrum for various sounding types, calculating the probabilities of detection (PODs) for several hundred observed soundings associated with the various forms of precipitation, and performing sensitivity studies of the effects of changing the degree of riming (f_{rim}), choice of T_{ice}, and DSD. We also demonstrate the effects of model uncertainty on the algorithm performance through consideration of plan views of precipitation type as well as sensitivity experiments.

c. Functional description of the SBC

The first step in the algorithm is to determine the top of the cloud. In the natural environment, one could declare this as the topmost layer with RH $\geq$ 100%. However, numerical weather prediction models that use a cumulus parameterization scheme may have some precipitation generated in subsaturated grid boxes. Common RH thresholds used to specify the potential for saturation in mesoscale models range from 70% to 80%. However, using such low thresholds will overestimate the cloud depth in grid boxes that are saturated, potentially biasing the classifier toward PL or SN (Rauber et al. 2001). To avoid this, if the column-maximum RH is greater than 80%, the cloud top is set to the layer with the highest RH. Otherwise, a simple classification of RA or SN is made depending on whether the surface T_w is greater or less than 0°C. This method allows for instances where hydrometeors generated at upper levels, in a completely glaciated portion of the cloud, act to seed lower cloud decks (e.g., Rauber et al. 2014; Stark et al. 2013).
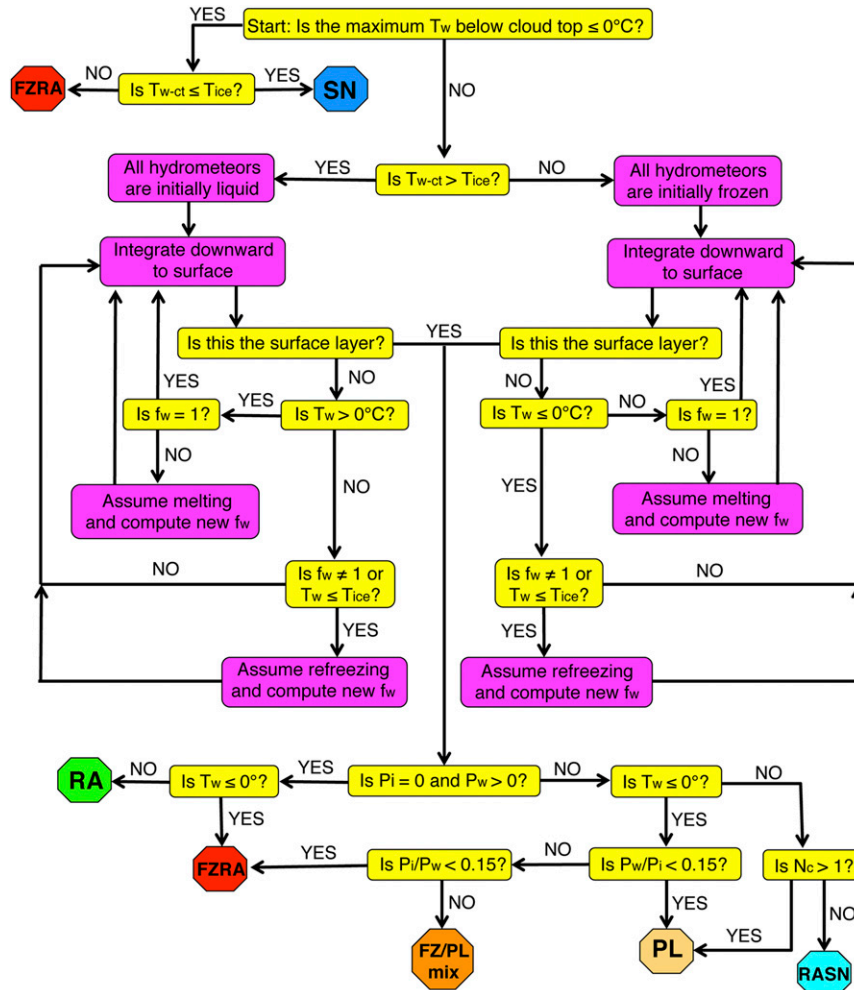
FIG. 2. A flowchart showing the logic used by the SBC. In the SBC, T_w, T_{ice}, T_{w-ct}, f_w, P_i, P_w, and N_c are the wet-bulb temperature; ice-nucleation temperature; wet-bulb temperature at cloud top; liquid-water fraction; precipitation rates of ice and liquid water, respectively; and the number of crossings that the T_w profile makes with the 0°C isotherm.

The algorithm then follows the flow chart depicted in Fig. 2. If the sounding is completely subfreezing below the cloud top and has $T_{w-ct} \leq T_{ice}$, it is classified as SN. Otherwise, FZRA is diagnosed. Those profiles that are not completely subfreezing have the liquid-water fraction f_w of each hydrometeor in a spectrum of sizes calculated at each model level from the cloud top to the surface. If $T_{w-ct} > T_{ice}$, all hydrometeors are assumed to be liquid at the cloud top. Otherwise, they are assumed to be frozen. At each model level, if $T_w > 0°C$ and $f_w < 1$ (i.e., there exists some ice in the hydrometeor), melting is assumed. For this, the equations used to compute f_w follow those presented in Trömel et al. (2014; see their appendix). Refreezing happens when either $T_w \leq T_{ice}$ or when the hydrometeor is composed of both liquid and ice *and* $T_w < 0°C$. The equations used to compute f_w in

refreezing layers follow those in Kumjian et al. (2012). The hydrometeor size bins are determined in such a way that the melted diameters of hydrometeors D_w in the jth bin are centered at $D_w = 0.05 + j\Delta D_w$ for $(j = 0, \ldots, n)$ where the bin size ΔD_w is 0.1 mm and n is the number of bins imposed by the user.

At the surface, the hourly precipitation rates for liquid water and ice P_w and P_i (mm h^{-1}) are computed according to

$$P_w = \frac{3600}{\rho_w} \sum_{D_{min}}^{D_{max}} m(D) f_w(D) V_T(D) N(D) \, dD \quad \text{and} \quad (1)$$

$$P_i = \frac{3600}{\rho_i} \sum_{D_{min}}^{D_{max}} m(D)[1 - f_w(D)] V_T(D) N(D) \, dD, \quad (2)$$
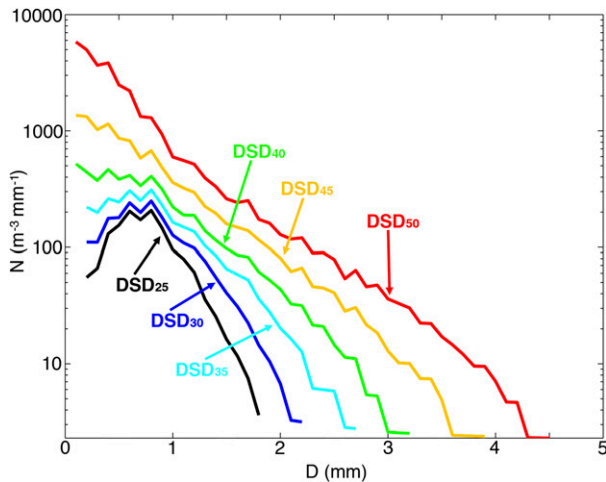
FIG. 3. The DSDs used to test SBC sensitivity. These are based on disdrometer measurements presented in Schuur et al. (2005) and are associated with precipitation systems with reflectivities ranging from 25 to 50 dBZ.

where 3600 is the number of seconds per hour; ρ_w and ρ_i are the densities of water and ice (g cm^{-3}), respectively; and $m(D)$, $f_w(D)$, $V_T(D)$, and $N(D)$ are, respectively, the mass (kg), liquid water fraction, terminal velocity (m s^{-1}), and size distribution (m^{-3}) of a hydrometeor with diameter D (mm). If $P_i = 0$ mm h^{-1} and $P_w > 0$ mm h^{-1}, then the precipitation is classified as either RA or FZRA (if surface $T_w < 0°$C). Those hydrometeors that are still unassigned are classified as FZRA, PL, FZRAPL, or RASN, depending on the ratios of P_i to P_w and the number of crossings the T_w profile makes with the 0°C isotherm (N_c), as indicated in Fig. 2.

One important note is that, although the SBC explicitly treats the processes of melting and refreezing, some simplifications are required for the code to be computationally efficient enough to be run in real time. For example, no interaction between particles, such as collision or aggregation, is accounted for. Processes that act to grow or deplete hydrometeors, such as condensation or evaporation, are also neglected. In other words, one hydrometeor aloft produces one hydrometeor at the surface with an unchanged D_w. Also, ice nucleation is assumed to occur at a prescribed temperature regardless of the hydrometeor size [laboratory experiments suggest larger drops begin freezing at warmer temperatures than smaller drops (Pruppacher and Klett 1997)]. This latter assumption may only be applicable in convective updrafts wherein larger raindrops have a higher likelihood of having an ice nucleus inside and, as a result, may nucleate faster at warmer temperatures. In the case of melting and refreezing, all raindrops are prenucleated regardless of their size. As is demonstrated in subsequent sections, despite these simplifications, the

SBC still provides a reasonably robust classification that is superior to existing algorithms.

d. Classification of select soundings

We now demonstrate how the SBC operates using select soundings that are associated with various forms of precipitation. For the following, a T_{ice} of $-6°$C and the DSD labeled as DSD$_{25}$ in Fig. 3 are used. This DSD comes from disdrometer measurements made in central Oklahoma over 7 yr for precipitation events associated with radar-observed reflectivities ranging from 20 to 30 dBZ (Schuur et al. 2005). This DSD has 18 size bins with a maximum D_w of 1.84 mm. Also, no riming on particles entering the melting layer is assumed. The sensitivity to each of these parameters will be discussed in section 3b.

1) CLASSIFICATION OF ICE PELLETS

Two examples in which PL are diagnosed by the SBC are presented. The first occurs at 0000 UTC 5 March 2008 at Buffalo, New York (BUF; see Fig. 5 for sounding locations). This sounding has an elevated warm layer capping a deep, cold subfreezing layer (Fig. 4a). The f_w, according to the SBC, as a function of height above ground level (AGL) and D_w, shows that all hydrometeors completely melt in the melting layer (i.e., $f_w = 1$; Fig. 4b). When the liquid water drops descend below 1 km AGL, where the ambient T_w is less than T_{ice}, ice nucleation and refreezing occur. The smallest hydrometeors almost instantly refreeze while larger ones refreeze more slowly.[1] In this example, since all hydrometeors completely refreeze before reaching the ground, PL is diagnosed.

The sounding for the other event has a very shallow melting layer and only those hydrometeors with D_w less than about 0.55 mm completely melt (Figs. 4c,d). Because $T_w > T_{ice}$ in the surface-based subfreezing layer, these drops do not refreeze before reaching the ground. However, the larger hydrometeors are able to refreeze because they only partially melted aloft. This yields a $P_w/P_i < 0.15$ and PL is diagnosed. For both examples, nearby surface observations indicate PL, in agreement with the SBC.

2) CLASSIFICATION OF FREEZING RAIN

Two examples of a FZRA diagnosis are also provided. The first has a deep elevated warm layer in which all hydrometeors completely melt (Figs. 4e,f). Because

---

[1] The time required for refreezing has been compared with explicit computations using equations from Pruppacher and Klett (1997) and shows good agreement.
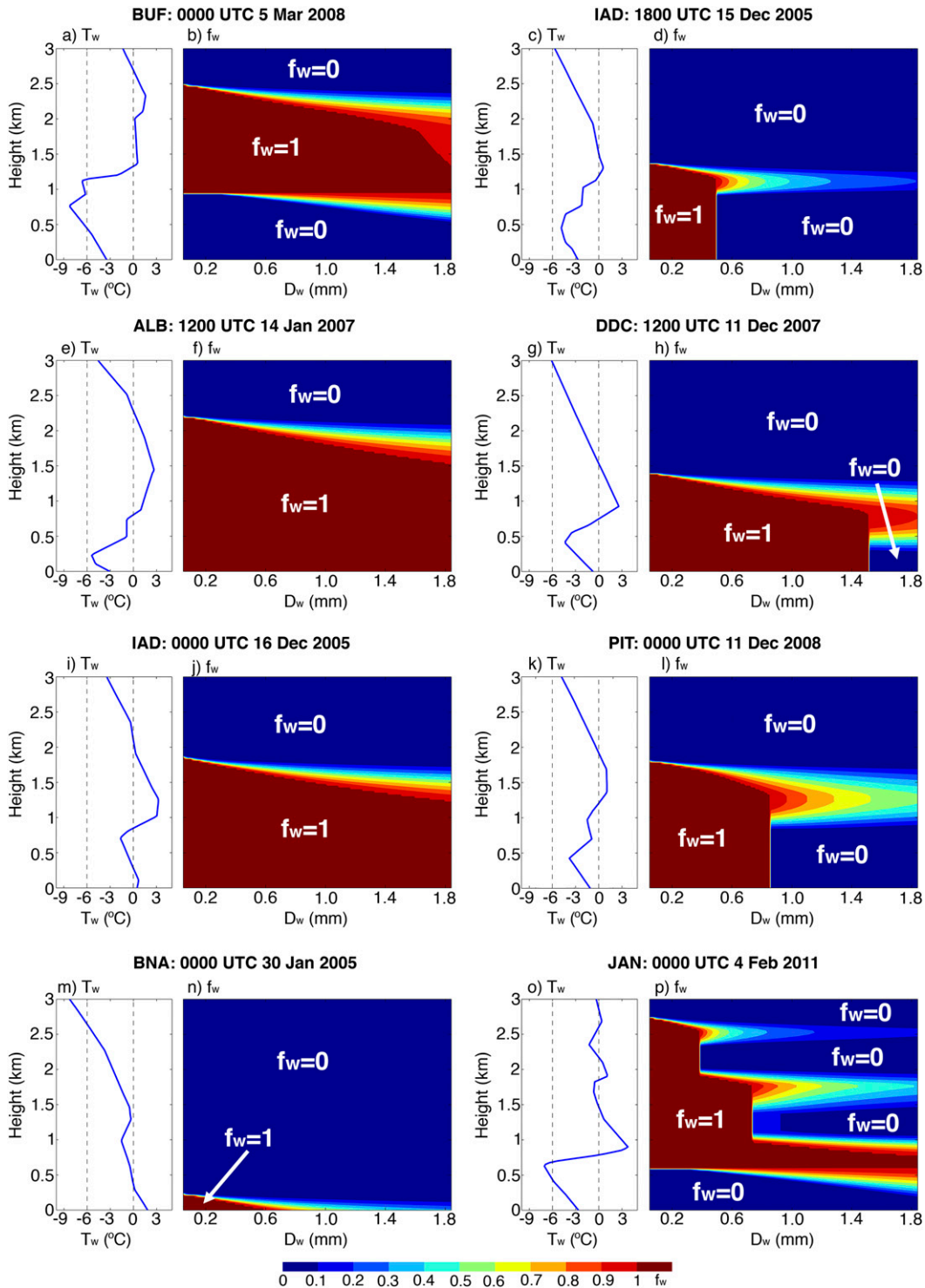
FIG. 4. The (a),(c),(e),(g),(i),(k),(m),(o) observed T_w profiles from select events, and (b),(d),(f),(h),(j),(l),(n),(p) the associated distribution of f_w as a function of D_w (shaded).

$T_w > T_{ice}$ in the surface-based subfreezing layer, no ice nucleation and, hence, no refreezing occur. Therefore, FZRA is diagnosed. In the other example, the melting layer is not as pronounced and hydrometeors with $D_w > 1.55$ mm only partially melt and, hence, are able to refreeze. Smaller hydrometeors completely melt aloft and remain as all liquid to the surface because the subfreezing layer is too warm for ice nucleation. This leads to a $P_i/P_w < 0.15$ and FZRA is diagnosed. Both diagnoses are consistent with surface observations taken coincident with the soundings.

3) CLASSIFICATION OF RAIN

Here, the classification is straightforward. If the surface $T_w > 0°C$ and the ratio $P_i/P_w < 0.15$, RA is diagnosed; otherwise, PL is the choice. Figure 4i is an example sounding that is classified as RA. It has a shallow surface-based warm layer that extends to about 200 m AGL. There is also a pronounced elevated warm layer. All hydrometeors completely melt in this layer (Fig. 4j). Although T_w is subfreezing between 600 and 740 m AGL, $T_w > T_{ice}$; hence, there is no refreezing. Because the surface $T_w > 0°C$, a RA classification is made, consistent with nearby surface observations.

4) CLASSIFICATION OF MIXES

FZRAPL is diagnosed when the number of crossings the T_w profile makes when the 0°C isotherm is more than one ($N_c > 1$; i.e., there is an elevated warm layer) and both P_i/P_w and P_w/P_i are greater than 0.15. An example is shown in Fig. 4k. The sounding has an elevated warm layer capping a surface-based subfreezing layer. The minimum T_w in this layer is greater than T_{ice}. Therefore, those hydrometeors with $D_w < 0.85$ mm, which completely melt in the melting layer, retain $f_w = 1$ to the surface (Fig. 4l). Larger hydrometeors only partially melt aloft and, therefore, completely refreeze in the subfreezing layer. This results in near-equal P_i and P_w, and FZRAPL is diagnosed.

An example of a profile conducive to RASN is shown in Fig. 4m. This sounding has a very shallow surface-based warm layer. For hydrometeors with $D_w < 0.6$ mm, there is complete melting in this layer, but most hydrometeors only partially melt and hit the ground as wet SN (Fig. 4n).

5) CLASSIFICATION OF COMPLEX SOUNDINGS

Profiles with multiple elevated warm layers, such as that shown in Fig. 4o, can exist. Such soundings can be quite difficult for classifiers that assume only one elevated warm layer can exist (i.e., Baldwin et al. 1994; Bourgouin 2000; Schuur et al. 2012). The SBC, since it explicitly calculates f_w at each level, can handle such
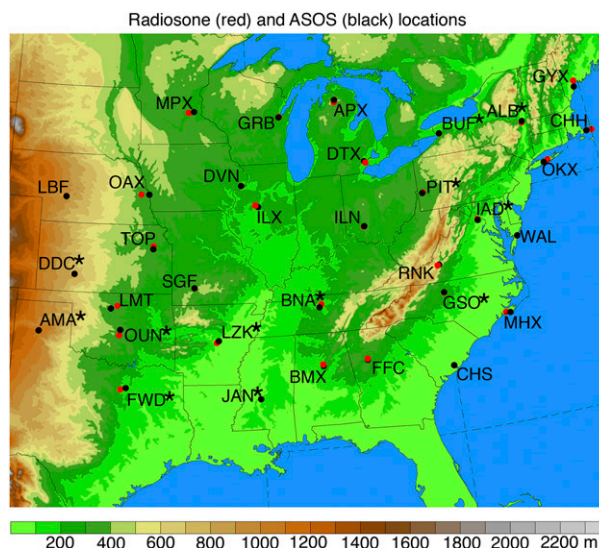

FIG. 5. The terrain (shaded) and location of radiosonde (black) and ASOS (red) sites used to select the events. The stations indicated with an asterisk are those that are routinely augmented.

soundings with reasonable accuracy. The manner in which hydrometeors with differing D_w melt and refreeze as they encounter each layer in the atmosphere is exhibited in Fig. 4p. The smaller hydrometeors have complete melting in the layers with $T_w > 0°C$ and complete refreezing in the layers with $T_w < T_{ice}$. Larger hydrometeors have only partial melting until they reach the lowest melting layer, where complete melting occurs. There is complete refreezing in the lowest subfreezing layer for all hydrometeor sizes. Hence, PL is diagnosed. This is consistent with the surface observations of precipitation type near the sounding.

3. Demonstration of SBC performance

a. Statistical performance of the SBC

The SBC is applied to a collection of observed soundings associated with SN, RA, PL, and FZRA. This dataset is the same as that used in Reeves et al. (2014) and is created by considering all soundings for winter months (i.e., October–March) from 2002 to 2013 for the sites shown in Fig. 5. Only those soundings whose precipitation type does not change during the 40-min window surrounding the launch time are considered. Additionally, no mixes are included. Finally, all soundings are required to ascend to at least 5 km AGL. This yields 649 SN, 545 RA, 422 FZRA, and 125 PL soundings. There are fewer PL soundings because this form of precipitation is only reported at stations that are augmented by human observers (indicated in Fig. 5). The data were manually quality controlled to remove soundings

TABLE 1. PODs (%) for the SBC algorithm (top and bottom rows) and from the five algorithms studied in Reeves et al. (2014) using observed soundings. For those cells with two values, the second corresponds to the score if one assumes a mix is a hit.

	SN	RA	FZRA	PL
SBC	91.4/95.2	97.2/98.3	62.4/72.8	63.2/73.6
Baldwin1	86.7	96.1	28.4	89.6
Baldwin2	97.1	96.1	28.4	56.0
Bourgouin	92.6	96.1	48.8/55.7	50.4/60.0
NSSL	94.1	96.4	40.3/78.9	26.4/70.4
Ramer	94.9	99.6	65.4/66.1	25.6
SBC perturbed	87.8/93.2	92.8/94.5	43.26/49.0	62.9/68.7

associated with obvious errors in the precipitation type, such as reports of RA in the presence of a surface-based subfreezing layer. For additional details on how these soundings were selected and quality controlled, the reader is referred to Reeves et al. (2014).

The PODs for each category of precipitation are presented in Table 1. Other types of verification scores were considered, but the interpretation does not change. Therefore, we limit our presentation to only the POD. For SN and RA, the PODs are 91.4% and 97.2%, respectively. Including RASN as a hit increases the PODs to 95.2% and 98.3%. The SBC is less robust with the detection of FZRA and PL, having PODs of 62.4% and 63.2%, respectively, or 72.8% and 73.6%, if one includes FZRAPL as a hit. To put these numbers in perspective, the PODs for the five algorithms considered in Reeves et al. (2014), which were also applied to the same set of soundings, are included in Table 1. The SBC's greatest advantage is its comparatively high PODs for FZRA and PL. While other algorithms may have a higher POD for one or the other of these classes, no other algorithm performs as well with *both* FZRA and PL.

b. Sensitivity to certain parameters

As suggested in section 2a, f_{rim}, T_{ice}, and the DSD may exert a nonnegligible control on the surface precipitation type. In the above analyses, prescribed values for each have been used. But some sensitivity does exist. These are quantified and discussed below.

1) SENSITIVITY TO THE DEGREE OF RIMING

The f_{rim} affects the particle diameter D and the density of snow ρ_s, which, in turn, alter the volume and terminal velocity of the frozen hydrometeors. These, then, affect the amount of time required for complete melting. One can account for variations in f_{rim} as follows:

$$D = 2.29 f_{rim}^{-0.48} D_w^{1.443} \quad \text{and} \tag{3}$$

$$\rho_s = 0.178 f_{rim} D^{-0.922}. \tag{4}$$

The units of D, D_w, and ρ_s are millimeters, millimeters, and grams per centimeter cubed, respectively. Both (3) and (4) come from Zawadzki et al. (2005) and assume f_{rim} ranges from 1 to 5, where 1 indicates no riming and 5 is for lump graupel. Let us consider the effects of changing f_{rim} for the sounding shown in Fig. 6a. This sounding has a pronounced elevated warm layer and an approximately 1-km-deep surface-based cold layer with a minimum T_w of about −5°C. All hydrometeors completely melt in the melting layer when $f_{rim} = 1$ (Fig. 6b), but hydrometeors with $D_w > 1.4$ mm only partially melt when $f_{rim} = 5$ (Fig. 6c). The final classification when $f_{rim} = 1$ is obviously FZRA, as all hydrometeors have an $f_w = 1$ at the surface. However, since less than 15% of the total water content is liquid at the surface for an $f_{rim} = 5$, a classification of PL is made. The actual observation indicates that only FZRA exists at this time and location. The SBC is run for all profiles discussed above with f_{rim} ranging from 1 to 5 and their PODs provided in Table 2. Increasing f_{rim} leads to decreased PODs for FZRA and increased PODs for PL (there is also a slight decrease in the PODs for RA). The most unbiased (i.e., the PODs for FZRA and PL are near equal) results occur for $f_{rim} = 1$.

2) SENSITIVITY TO THE ICE NUCLEATION TEMPERATURE

The choice of T_{ice} affects whether particles will be initialized as liquid or frozen at the cloud top and at what temperature refreezing can occur for hydrometeors that are all liquid. The sounding shown in Fig. 6d has a strong sensitivity to T_{ice}. Assuming $T_{ice} = −6°C$ allows for complete refreezing of almost all drops (Fig. 6e). Thus, a classification of PL is made. Decreasing it to −10°C does not change the rate of melting aloft (cf. Figs. 6e and 6f), but it implies that the portion of the sounding below 500 m AGL has temperatures greater than T_{ice} and so refreezing cannot occur, resulting in FZRA (Fig. 6f).

To explore the sensitivity to the choice of T_{ice}, the SBC is rerun for all profiles using a T_{ice} ranging from −15° to 0°C. The resulting PODs are provided in Table 3. The PODs for SN decrease with decreasing T_{ice} because more soundings have $T_{w–ct} > T_{ice}$ and are consequently classified as FZRA. The PODs for FZRA and PL are inversely sensitive to T_{ice}. However, both have a POD of about 62% for a T_{ice} of −6°C. Other values of T_{ice} bias the PODs toward one or the other form of precipitation, thus justifying the choice of $T_{ice} = −6°C$ throughout the paper.

3) SENSITIVITY TO THE DROP SIZE DISTRIBUTION

To test the effects of changing the DSD, the SBC is rerun using the array of DSDs shown in Fig. 3. These are
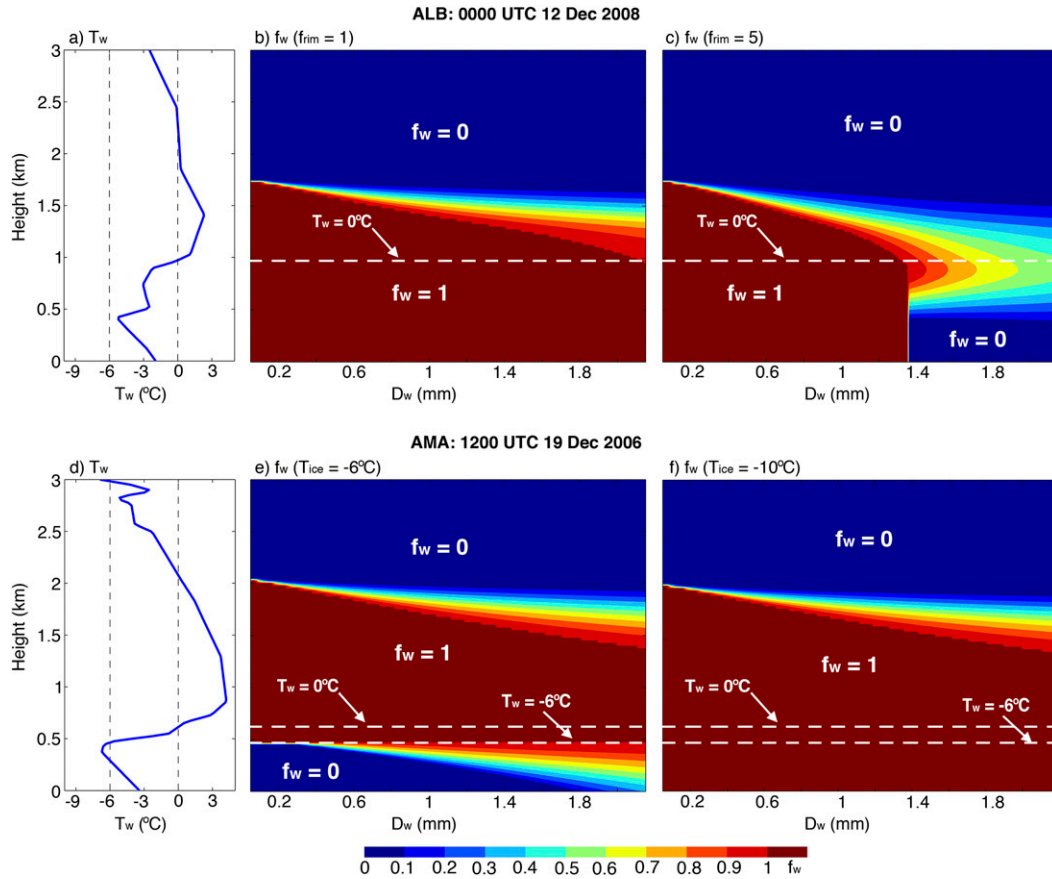
FIG. 6. The (a),(d) observed T_w profile, with associated f_w profiles assuming an f_{rim} = (b) 1 or (c) 5 and a T_{ice} = (e) −6° or (f) −10°C.

from observations presented in Schuur et al. (2005) and are associated with precipitation systems with reflectivities ranging from 25 to 50 dBZ. Some of these values are higher than those typically observed in a wintertime precipitation system, but their use herein demonstrates the sensitivity. The PODs for the different DSDs is provided in Table 4. SN is not dependent on the choice of DSD and RA is only slightly dependent on it. Even FZRA and PL are not especially dependent on the DSD. Both decrease as the reflectivity increases while the fraction of FZRAPL classifications increase. Several other hypothetical DSDs were also considered (not shown). These indicate that the PODs are only slightly dependent on the choice of DSD.

c. Examples from select events

Plan views of the horizontal distribution of precipitation type illustrate the algorithm's ability to correctly distribute the various forms of precipitation. Figures 7a,c,e show the observed precipitation type according to the meteorological Phenomena Identification Near the Ground (mPING; Elmore et al. 2014) dataset for the 2-h

period surrounding the time indicated. These observations are collected by citizen observers and are not quality controlled. However, analyses in Elmore et al. (2014, 2015) suggest they are sufficiently accurate for this type of inquiry.

The events are from three different types of weather systems. The first is associated with a strong nor'easter in the North Atlantic states (Griffin et al. 2014; Picca et al. 2014; Fig. 7a). A narrow transition zone with various forms of precipitation including FZRA, RASN, and PL is evident over Long Island and central New Jersey.

TABLE 2. PODs (%) for the SBC algorithm using observed soundings and an f_{rim} ranging from 1 to 5. The second value in each cell corresponds to the score if one assumes a mix is a hit.

f_{rim}	SN	RA	FZRA	PL
1	91.4/95.2	97.2/98.3	62.4/72.8	63.2/73.6
2	91.4/95.2	96.3/97.6	55.7/69.9	71.2/79.8
3	91.4/95.2	95.9/97.2	53.0/68.6	74.4/83.8
4	91.4/95.2	95.5/96.8	50.7/67.4	75.2/84.6
5	91.4/95.2	95.2/96.5	48.0/66.7	75.2/84.6

TABLE 3. PODs (%) for the SBC algorithm using observed soundings and a T_{ice} ranging from 0° to −15°C. The second value in each cell corresponds to the score if one assumes a mix is a hit.

T_{ice} (°C)	SN	RA	FZRA	PL
0	89.5/93.3	95.7/96.9	16.9/44.5	86.4/87.2
−1	89.5/93.3	95.7/96.9	17.9/47.7	84.8/86.4
−2	89.5/93.3	96.4/97.6	23.8/49.4	84.8/86.4
−3	89.5/93.3	96.8/98.0	34.7/53.6	80.0/84.8
−4	89.5/93.3	97.0/98.2	43.9/60.6	75.2/82.4
−5	90.9/94.7	97.0/98.2	54.5/69.2	69.3/77.6
−6	91.4/95.2	97.2/98.3	62.4/72.8	63.2/73.6
−7	91.2/95.1	97.2/98.3	66.6/83.3	59.2/72.8
−8	89.6/93.5	97.2/98.3	69.6/86.6	52.0/68.0
−9	87.9/91.7	97.2/98.3	71.1/89.3	47.2/67.2
−10	86.3/89.9	97.2/98.3	72.8/92.0	46.4/66.4
−11	83.7/87.4	97.2/98.3	75.0/94.5	42.4/65.6
−12	82.1/85.8	97.2/98.3	75.5/95.5	41.6/64.8
−13	78.7/82.4	97.2/98.3	76.0/96.0	39.2/64.8
−14	75.5/79.2	97.2/98.3	76.0/96.0	39.2/64.8
−15	70.3/73.9	97.2/98.3	76.0/96.0	39.2/64.8

TABLE 4. PODs (%) for the SBC algorithm using observed soundings and the DSDs shown in Fig. 6. The second value in each cell corresponds to the score if one assumes a mix is a hit. OBS refers to the DSD based on observed disdrometer measurements.

DSD	SN	RA	FZRA	PL
DSD_{25}	91.4/95.2	97.2/98.3	62.4/72.8	63.2/73.6
DSD_{30}	91.4/95.2	97.0/98.0	60.5/76.0	63.2/75.2
DSD_{35}	91.4/95.2	96.6/97.6	58.2/79.5	63.2/79.2
DSD_{40}	91.4/95.2	96.4/97.4	56.5/81.2	62.4/80.8
DSD_{45}	91.4/95.2	96.0/97.2	53.7/82.0	63.2/83.2
DSD_{50}	91.4/95.2	95.8/97.0	53.0/82.5	59.2/84.0

Mostly SN and RA are observed north and south of this zone, respectively. The second occurs in association with a warm front across the southern United States (Fig. 7c). Mostly RA is reported over the Gulf Coast states, Tennessee, and southern Kentucky. A mix of PL and FZRA is seen over Illinois, Indiana, and Ohio. PL is also observed over western North Carolina. In the upper Midwest, most reports are of SN. The last event occurs in association with cold-air damming along the Appalachian Mountains. Mostly SN is observed over regions of elevated terrain (Fig. 7e) and a mix of PL and FZRA is identified over the Piedmont region of North and South Carolina and northern Georgia and Alabama.

The SBC precipitation-type distributions are created using the Rapid Refresh (RAP; Brown et al. 2011) analyses of T_w, RH, and pressure. These have 51 terrain-following vertical levels and a 13-km grid spacing. The distributions are in fair agreement with the observations. For the first event, the SBC captures the position and width of the transition zone over Long Island and the presence of RA to the south and SN to the north (Fig. 7b). In the second, the aerial extents of the regions of SN, FZRA, IP, and RA are similarly sized to the observations, although some placement errors exist (Fig. 7d). In the last event, the SBC analysis correctly captures the location of the RA–FZRA transition zone over central Georgia and southern South Carolina and the presence of RASN over northern Alabama (Fig. 7f).

However, there are some important differences between the observations and the SBC analyses. For example, there is a region diagnosed as RASN over western Pennsylvania in Fig. 7b. The observations suggest some RA, PL, and FZRA cases are noted in this

area. In the second event, SN is diagnosed over northern Indiana and southwest Ohio that does not agree with mPING observations (cf. Figs. 7c and 7d). The region of FZRA is also too far south relative to the mPING observations. Over western North Carolina, the SBC indicates RASN rather than PL. Finally, in the third event, the SBC fails to diagnose PL over central North Carolina, instead indicating SN (Fig. 7f). In all three of these examples, the mPING observations suggest there is an elevated warm layer aloft that is not present in the RAP analyses. It is unclear whether the RAP model has failed to position the elevated warm layer far enough north or if the mPING users are making errant reports, but inasmuch as the model analyses and observations are consistent with each other, the SBC faithfully represents the precipitation type.

d. Effects of model uncertainty

Now that we have seen how the SBC performs for observed soundings and the types of distributions it yields, let us consider the effects of model uncertainty. Herein, we use the perturbed soundings from Reeves et al. (2014). These are generated by perturbing the observed soundings described above 1000 times each in accordance with the range of uncertainty inherent in a mesoscale model. The error distribution has a higher concentration near 0°C and is approximately Gaussian in nature. The reader is referred to Reeves et al. (2014) for more information on this sounding dataset.

The PODs for the perturbed soundings are included in Table 1 (cf. top and bottom rows). For SN, RA, and PL, the PODs decrease by only a few percentage points, indicating that the SBC is quite robust for these categories, even in the face of typical model uncertainty. However, the decrease in POD for FZRA is quite large, about 20%. This merits some explanation. Many of the observed FZRA soundings have elevated warm layers that are not warm enough to support complete melting of all hydrometeors or have surface-based cold layers with minimum T_w that are only slightly warmer than T_{ice} (Reeves et al. 2014; see their Figs. 3b,d). Small
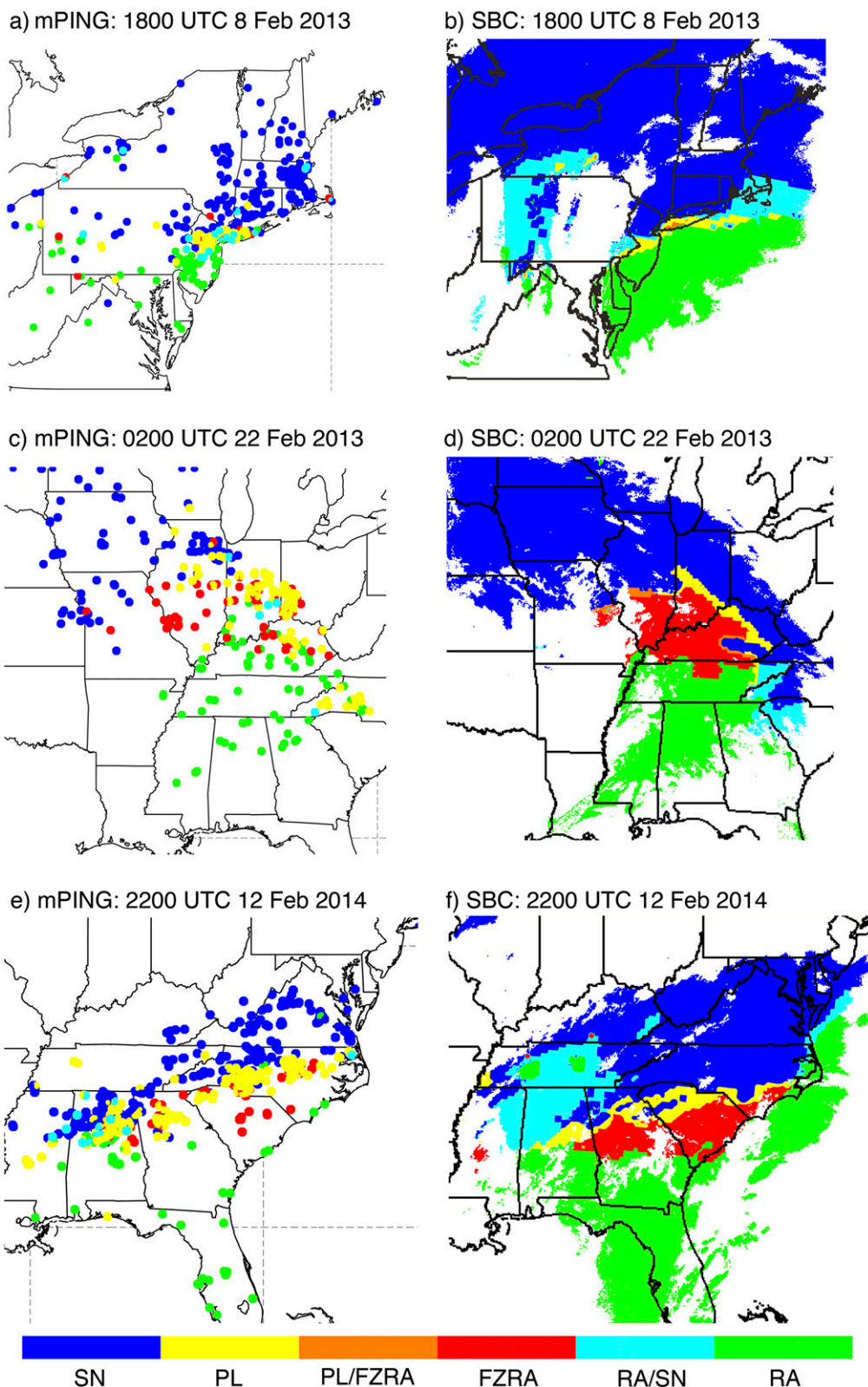
FIG. 7. The (a),(c),(e) mPING distributions of observed precipitation type for the 2-h period surrounding the time indicated at the top of each panel, and (b),(d),(f) the corresponding SBC analyses. In (b),(d), and (f) only the areas with observed composite reflectivity greater than 0 dBZ are shaded.
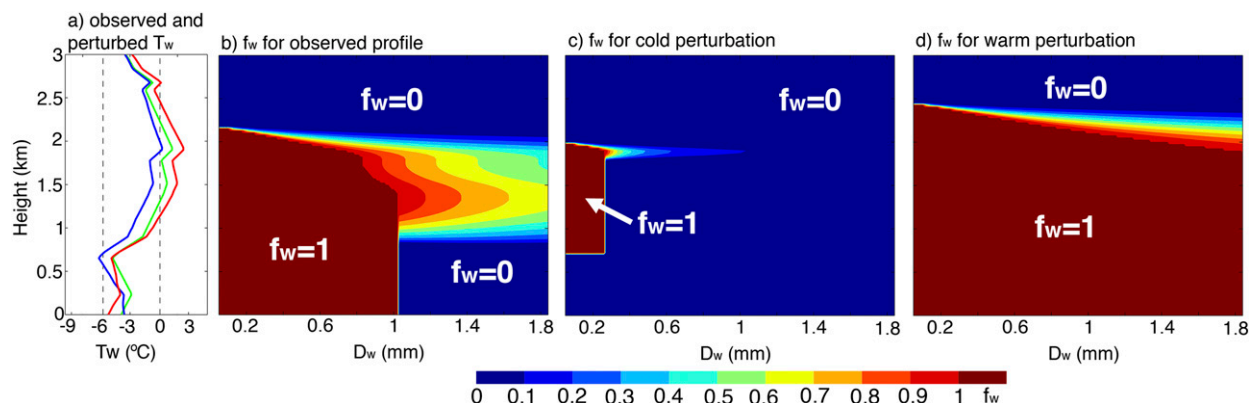
FIG. 8. The (a) observed (green) and select perturbed (cold, blue; warm, red) T_w profiles at 1200 UTC 12 Jan 2005 at Albany, New York (ALB), and (b)–(d) their associated f_w distributions.

perturbations in either the warm or cold direction are often sufficient to cause either incomplete melting aloft or to trigger ice nucleation at low levels as is demonstrated for the soundings shown in Fig. 8a. The observed T_w profile (given by the green curve) has a shallow elevated warm layer between 1400 and 2300 m AGL. The minimum T_w in the surface-based cold layer is greater than T_{ice}. In the observed sounding, hydrometeors with $D_w < 1$ mm completely melt aloft and do not refreeze before hitting the ground (Fig. 8b). Larger hydrometeors only partially melt aloft and so do refreeze before reaching the ground. This sounding is classified as FZRAPL. Comparatively cold and warm perturbations (given by the blue and red curves, respectively) are included in Fig. 8a. These have different depths and maximum T_w in the elevated warm layer and different minimum T_w in the surface-based cold layer. In the cold perturbation, smaller hydrometeors still completely melt aloft, but refreeze in the layer with $T_w \leq T_{ice}$ (Fig. 8c). This sounding is classified as PL. In the warm perturbation, all hydrometeors melt in the elevated warm layer and do not refreeze in the surface-based cold layer because $T_w > T_{ice}$ (Fig. 8d). This sounding is classified as FZRA. The actual observed precipitation type at the surface is FZRA.

Discussions in Thériault et al. (2010) suggest the degree of uncertainty noted above is entirely reasonable for FZRA. Indeed, other classifiers have similar decreases in their FZRA PODs (Reeves et al. 2014). We note that the POD for the perturbed FZRA soundings is close to the variability in the natural environment, as discussed in Elmore et al. (2015) and may explain why soundings such as those in Fig. 8a are misclassified. A high degree of horizontal variability in precipitation type could signify that refreezing upon contact only occurs in favored locations, such as on elevated surfaces, away from buildings and roads, etc. Indeed, the National

Center for Environmental Information's Storm Events Database corroborates this assumption, describing the event as having light SN that transitions to "a mixture of freezing rain and sleet" and, eventually, "plain rain."

e. Mitigating the effects of uncertainty

The combined effects of these sources of uncertainty are significant enough to justify mitigative action. The steps one might take depend on whether the SBC is applied to a model analysis or forecast. If one is using an analysis, dual-polarized radar observations could be paired with the SBC to provide a reasonable estimate of f_{rim} as is discussed in Ryzhkov et al. (2016) and Vogel et al. (2015). A reasonable DSD may be assigned by following the methodology of Cao et al. (2008). They show that the Z_{dr} dependency on Z is positive for RA, negative for SN, and remains low and does not depend on Z for PL and graupel. The Z_{dr} slopes are also used to discriminate between SN/PL and FZRA in Trömel et al. (2016, manuscript submitted to *Meteor. Z.*). Finally, one can use the dual-polarized radar observations to confirm or refute the classification as in Schuur et al. (2012) or look for refreezing signatures in dual-polarized radar observations (Kumjian et al. 2013). The benefit of such an approach is that the surface classification can be updated each time a new radar mosaic is created (every 2–5 min). This has obvious value to certain sectors, such as the aviation industry.

However, if one is applying the SBC to forecast data, different steps must be taken. One could assign reasonable estimates of f_{rim} using the model-predicted mixing ratios for SN and graupel. The DSD could also be directly obtained from the microphysical parameterization scheme. The most obvious approach for addressing model uncertainty is to switch from a deterministic to a probabilistic frame of reference. This, of course, requires the use of ensemble modeling, which, at

present, is not operationally performed at higher resolutions. It is also possible to apply a probabilistic filter, such as is promoted in the recent work of Chenard et al. (2015). This work uses cumulative density functions of T_w in the lower troposphere to assign a probability to the different classes. Future work in this direction is strongly advocated.

4. Conclusions

A new surface precipitation-type classification algorithm is presented. This algorithm, referred to as the spectral bin classifier, diagnoses six categories of precipitation: RA, SN, FZRA, PL, RASN, and FZRAPL. It works by calculating the liquid-water fraction f_w of hydrometeors of different sizes as they descend from the cloud top to the surface. The relative precipitation rates of frozen and unfrozen content (P_i and P_w, respectively) are then computed and used to determine the type of precipitation at the surface. The rates of melting and refreezing are explicitly calculated, but the algorithm does not account for hydrometeors to interact or for hydrometeor-size-dependent ice nucleation. This allows the process to be computationally efficient enough to run in real time.

Unlike other approaches (e.g., Baldwin et al. 1994; Bourgouin 2000; Ramer 1993; Schuur et al. 2012), the use of multiple size bins allows one to make assumptions about the total hydrometeor content that is refrozen or melted at a given layer in the atmosphere. Analyses of f_w as a function of hydrometeor size clearly show the relative quickness of the melting and refreezing of smaller hydrometeors compared to larger ones. Thus, it can be more definitively stated whether complete or partial melting has occurred aloft. As a result, the distinction between FZRA and PL is made clearer than in more conventional algorithms.

The SBC was applied to a collection of 1741 observed soundings associated with SN, RA, FZRA, and PL. The classifier performs very well with the detection of SN and RA, having PODs that range from 91.4% to 98.3%. Although the PODs are somewhat less for FZRA and PL (61.6%–73.6%), comparison of the SBC detection to that from existing algorithms shows that the SBC has greater accuracy. Plan views from select events show that inasmuch as the model data accurately represent the actual thermodynamic profiles, the SBC reliably captures the distribution of precipitation types at the surface.

The effects of various sources of uncertainty on the classifier's performance were quantified. The SBC is sensitive to the choice of DSD, amount of riming above the melting layer, and the choice of T_{ice}. All of these

have inverse effects on the PODs for FZRA and PL. Model uncertainty was also examined. This was accomplished by perturbing the observed soundings 1000 times each in accordance with the range of uncertainty inherent in a mesoscale model. The SBC is fairly immune to uncertainty effects for SN, RA, and PL. However, FZRA PODs were considerably degraded by model uncertainty. This is due to the fact that many FZRA events have elevated warm layers that are unable to support complete melting of all hydrometeors or that have a surface-based cold layer minimum T_w that is close to T_{ice}. Small perturbations are often sufficient to prevent a large fraction of the hydrometeors from melting aloft or to allow for complete refreezing before reaching the ground.

Certain steps are recommended to address the issue of uncertainty. If one is applying the SBC to a model analysis, dual-polarized radar observations can be used to assign a reasonable f_{rim} and DSD. Radar observations can also be used to confirm or refute the SBC output, thus allowing for greater certainty in the analysis, especially in the cases of melting or refreezing. If one is applying the SBC to a model forecast, the f_{rim} and DSD can be gleaned from the microphysical parameterization scheme. Ensemble forecasting can alleviate issues with model uncertainty. However, we note that even without these measures, the SBC provides more reliable classifications than other existing methods.

REFERENCES

Baldwin, M., R. Treadon, and S. Contorno, 1994: Precipitation type prediction using a decision tree approach with NMC's mesoscale eta model. Preprints. *10th Conf. on Numerical Weather Prediction*, Portland, OR, Amer. Meteor. Soc., 30–31.

Benjamin, S. G., J. M. Brown, and T. G. Smirnova, 2016: Explicit precipitation-type diagnosis from a model using a mixed-phase bulk cloud–precipitation microphysics parameterization. *Wea. Forecasting*, **31**, 609–619, doi:10.1175/WAF-D-15-0136.1.

Bernstein, B. C., 2000: Regional and local influences on freezing drizzle, freezing rain, and ice pellet events. *Wea. Forecasting*, **15**, 485–508, doi:10.1175/1520-0434(2000)015<0485: RALIOF>2.0.CO;2.

Bourgouin, P., 2000: A method to determine precipitation type. *Wea. Forecasting*, **15**, 583–592, doi:10.1175/1520-0434(2000)015<0583:AMTDPT>2.0.CO;2.

Brown, J. M., and Coauthors, 2011: Improvement and testing of WRF physics options for application to Rapid Refresh and High Resolution Rapid Refresh. Preprints, *14th Conf. on Mesoscale Processes/15th Conf. on Aviation, Range, and Aerospace Meteorology*, Los Angeles, CA, Amer. Meteor. Soc., 5.5. [Available online at https://ams.confex.com/ams/14Meso15ARAM/webprogram/Paper191234.html.]

Cao, Q., G. Zhang, E. Brandes, T. Schuur, A. Ryzhkov, and K. Ikeda, 2008: Analysis of video disdrometer and polarimetric radar data to characterize rain microphysics in Oklahoma. *J. Appl. Meteor. Climatol.*, **47**, 2238–2255, doi:10.1175/2008JAMC1732.1.

Changnon, S. A., 2003: Urban modification of freezing-rain events. *J. Appl. Meteor.*, **42**, 863–870, doi:10.1175/1520-0450(2003)042<0863:UMOFE>2.0.CO;2.

Chenard, M., P. N. Schumacher, and H. D. Reeves, 2015: Determining precipitation type from maximum temperature in the lower atmosphere. *Proc. 27th Conf. on Weather Analysis and Forecasting/23rd Conf. on Numerical Weather Prediction*, Chicago, IL, Amer. Meteor. Soc., 6B.2. [Available online at https://ams.confex.com/ams/27WAF23NWP/webprogram/Paper273342.html.]

Cortinas, J. V., Jr., 2000: A climatology of freezing rain in the Great Lakes region of North America. *Mon. Wea. Rev.*, **128**, 3574–3588, doi:10.1175/1520-0493(2001)129<3574:ACOFRI>2.0.CO;2.

——, B. C. Bernstein, C. C. Robbins, and J. W. Strapp, 2004: An analysis of freezing rain, freezing drizzle, and ice pellets across the United States and Canada: 1976–1990. *Wea. Forecasting*, **19**, 377–390, doi:10.1175/1520-0434(2004)019<0377:AAOFRF>2.0.CO;2.

Crawford, R. W., and R. E. Stewart, 1995: Precipitation type characteristics at the surface in winter storms. *Cold Reg. Sci. Technol.*, **23**, 215–229, doi:10.1016/0165-232X(94)00014-O.

Czys, R., R. Scott, K. C. Tang, R. W. Przybylinski, and M. E. Sabones, 1996: A physically based, nondimensional parameter for discriminating between freezing rain and ice pellets. *Wea. Forecasting*, **11**, 591–598, doi:10.1175/1520-0434(1996)011<0591:APBNPF>2.0.CO;2.

Elmore, K. L., Z. L. Flamig, V. Lakshmanan, B. T. Kaney, H. D. Reeves, V. Farmer, and L. P. Rothfusz, 2014: mPING: Crowdsourcing weather reports for research. *Bull. Amer. Meteor. Soc.*, **95**, 1335–1342, doi:10.1175/BAMS-D-13-00014.1.

——, H. Moser, D. Apps, and H. D. Reeves, 2015: Evaluation of precipitation type forecasts by three operational models. *Wea. Forecasting*, **30**, 656–667, doi:10.1175/WAF-D-14-00068.1.

Griffin, E. M., T. J. Schuur, A. V. Ryzhkov, H. D. Reeves, and J. C. Picca, 2014: A polarimetric and microphysical investigation of the Northeast blizzard of 8–9 February 2013. *Wea. Forecasting*, **29**, 1271–1294, doi:10.1175/WAF-D-14-00056.1.

Ikeda, K., M. Steiner, J. Pinto, and C. Alexander, 2013: Evaluation of cold-season precipitation forecasts generated by the hourly updating High-Resolution Rapid Refresh model. *Wea. Forecasting*, **28**, 921–939, doi:10.1175/WAF-D-12-00085.1.

Kumjian, M. R., S. M. Ganson, and A. V. Ryzhkov, 2012: Freezing of raindrops in deep convective updrafts: A microphysical and polarimetric model. *J. Atmos. Sci.*, **69**, 3471–3490, doi:10.1175/JAS-D-12-067.1.

——, A. V. Ryzhkov, H. D. Reeves, and T. J. Schuur, 2013: A dual-polarized radar signature of hydrometeor refreezing in winter

storms. *J. Appl. Meteor. Climatol.*, **52**, 2549–2566, doi:10.1175/JAMC-D-12-0311.1.

Manikin, G. S., 2005: An overview of precipitation type forecasting using NAM and SREF data. Preprints, *21st Conf. on Weather Analysis and Forecasting/17th Conf. on Numerical Weather Prediction*, Washington, DC, Amer. Meteor. Soc., 8A.6. [Available online at https://ams.confex.com/ams/WAFNWP34BC/techprogram/paper_94838.htm.]

——, K. F. Brill, and B. Ferrier, 2004: An Eta Model precipitation type mini-ensemble for winter weather forecasting. Preprints, *20th Conf. on Weather Analysis and Forecasting/16th Conf. on Numerical Weather Prediction*, Seattle, WA, Amer. Meteor. Soc., 23.1. [Available online at https://ams.confex.com/ams/84Annual/techprogram/paper_73517.htm.]

Meyers, M. P., P. J. DeMott, and W. R. Cotton, 1992: New primary ice-nucleation parameterization in an explicit cloud model. *J. Appl. Meteor.*, **31**, 708–721, doi:10.1175/1520-0450(1992)031<0708:NPINPI>2.0.CO;2.

Petters, M. D., and T. P. Wright, 2015: Revisiting ice nucleation from precipitation samples. *Geophys. Res. Lett.*, **42**, 8758–8766, doi:10.1002/2015GL065733.

Picca, J. C., D. M. Schultz, B. A. Colle, S. Ganetis, D. R. Novak, and M. Sienkiewicz, 2014: The value of dual-polarization radar in diagnosing the complex microphysical evolution of an intense snowband. *Bull. Amer. Meteor. Soc.*, **95**, 1825–1834, doi:10.1175/BAMS-D-13-00258.1.

Pruppacher, H. R., and J. D. Klett, 1997: *Microphysics of Clouds and Precipitation*. Kluwer Academic, 954 pp.

Ralph, F. M., and Coauthors, 2005: Improving short-term (0–48 h) cool-season quantitative precipitation forecasting: Recommendations from a USWRP workshop. *Bull. Amer. Meteor. Soc.*, **86**, 1619–1632, doi:10.1175/BAMS-86-11-1619.

Ramer, J., 1993: An empirical technique for diagnosing precipitation type from model output. Preprints, *Fifth Int. Conf. on Aviation Weather Systems*, Vienna, VA, Amer. Meteor. Soc., 227–230.

Rauber, R. M., L. S. Olthoff, and M. K. Ramamurthy, 2000: The relative importance of warm rain and melting processes in freezing precipitation events. *J. Appl. Meteor.*, **39**, 1185–1195, doi:10.1175/1520-0450(2000)039<1185:TRIOWR>2.0.CO;2.

——, ——, ——, and K. E. Kunkel, 2001: Further investigation of a physically based, nondimensional parameter for discriminating between locations of freezing rain and ice pellets. *Wea. Forecasting*, **16**, 185–191, doi:10.1175/1520-0434(2001)016<0185:FIOAPB>2.0.CO;2.

——, M. K. Macomber, D. M. Plummer, A. A. Rosenow, G. M. McFarquhar, B. F. Jewett, D. Leon, and J. M. Keeler, 2014: Finescale radar and airmass structure of the comma head of a continental winter cyclone: The role of three airstreams. *Mon. Wea. Rev.*, **142**, 4207–4229, doi:10.1175/MWR-D-14-00057.1.

Reeves, H. D., K. L. Elmore, A. Ryzhkov, T. Schuur, and J. Krause, 2014: Source of uncertainty in precipitation-type forecasting. *Wea. Forecasting*, **29**, 936–953, doi:10.1175/WAF-D-14-00007.1.

Robbins, C. C., and J. V. Cortinas Jr., 2002: Local and synoptic environments associated with freezing rain in the contiguous United States. *Wea. Forecasting*, **17**, 47–65, doi:10.1175/1520-0434(2002)017<0047:LASEAW>2.0.CO;2.

Ryzhkov, A. V., H. D. Reeves, J. Krause, and H. Burcham, 2014: Discrimination between winter precipitation types based on explicit microphysical modeling of melting and refreezing in the polarimetric hydrometeor classification algorithm. *Eighth European Conf. on Radar Meteorology*, Garmisch-Partenkirchen,

Germany, European Meteorological Society, MIC.P07. [Available online at http://www.pa.op.dlr.de/erad2014/programme/ExtendedAbstracts/198_Ryzhkov.pdf.]

——, P. Zhang, H. Reeves, M. Kumjian, T. Tschallener, S. Trömel, and C. Simmer, 2016: Quasi-vertical profiles a new way to look at polarimetric radar data. *J. Atmos. Oceanic Technol.*, **33**, 551–562, doi:10.1175/JTECH-D-15-0020.1.

Schuur, T. J., A. V. Ryzhkov, and D. R. Clabo, 2005: Climatological analysis of DSDs in Oklahoma as revealed by 2D-video disdrometer and polarimetric WSR-88D radar. Preprints, *32nd Conf. on Radar Meteorology*, Albuquerque, NM, Amer. Meteor. Soc., 15R.4. [Available online at https://ams.confex.com/ams/32Rad11Meso/techprogram/paper_95995.htm.]

——, H.-S. Park, A. V. Ryzhkov, and H. D. Reeves, 2012: Classification of precipitation types during transitional winter weather using the RUC model and polarimetric radar retrievals. *J. Appl. Meteor. Climatol.*, **51**, 763–779, doi:10.1175/JAMC-D-11-091.1.

Stark, D., B. Colle, and S. E. Yuter, 2013: Observed microphysical evolution for two East Coast winter storms and the associated snow bands. *Mon. Wea. Rev.*, **141**, 2037–2057, doi:10.1175/MWR-D-12-00276.1.

Stewart, R. E., J. M. Thériault, and W. Henson, 2015: On the characteristics of and processes producing winter precipitation types near 0°C. *Bull. Amer. Meteor. Soc.*, **96**, 623–639, doi:10.1175/BAMS-D-14-00032.1.

Thériault, J. M., and R. E. Stewart, 2010: A parameterization of the microphysical processes forming many types of winter precipitation. *J. Atmos. Sci.*, **67**, 1492–1508, doi:10.1175/2009JAS3224.1.

——, ——, and W. Henson, 2010: On the dependence of winter precipitation types and temperature, precipitation rate, and associated features. *J. Appl. Meteor. Climatol.*, **49**, 1429–1442, doi:10.1175/2010JAMC2321.1.

Thompson, G., R. M. Rasmussen, and K. Manning, 2014: Explicit forecasts of winter precipitation using an improved bulk microphysics scheme. Part I: Description and sensitivity analysis. *Mon. Wea. Rev.*, **132**, 519–542, doi:10.1175/1520-0493(2004)132<0519:EFOWPU>2.0.CO;2.

Trömel, S., A. V. Ryzhkov, P. Zhang, and C. Simmer, 2014: Investigations of backscatter differential phase in the melting layer. *J. Appl. Meteor. Climatol.*, **53**, 2344–2359, doi:10.1175/JAMC-D-14-0050.1.

Vogel, J. M., F. Fabry, and I. Zawadzki, 2015: Attempts to observe polarimetric signatures of riming in stratiform precipitation. *Proc. 37th Conf. on Radar Meteorology*, Norman, OK, Amer. Meteor. Soc., 6B.6. [Available online at https://ams.confex.com/ams/37RADAR/webprogram/Paper275246.html.]

Wandishin, M. S., M. E. Baldwin, S. L. Mullen, and J. V. Cortinas Jr., 2005: Short-range ensemble forecasts of precipitation type. *Wea. Forecasting*, **20**, 609–626, doi:10.1175/WAF871.1.

Zawadzki, I., W. Szyrmer, C. Bell, and F. Fabry, 2005: Modeling of the melting layer. Part III: The density effect. *J. Atmos. Sci.*, **62**, 3705–3723, doi:10.1175/JAS3563.1.